AFRL-AFOSR-VA-TR-2024-0156

LOCAL MULTIPHYSICS STUDIES OF EPOXY NANOCOMPOSITES FOR ELECTRONICS PACKAGING

Ioannis Chasiotis
UNIVERSITY OF ILLINOIS
506 S WRIGHT ST
URBANA, IL, 61801
USA

02/13/2024
Final Technical Report

DISTRIBUTION A: Distribution approved for public release.

Air Force Research Laboratory
Air Force Office of Scientific Research
Arlington, Virginia 22203
Air Force Materiel Command

REPORT DOCUMENTATION PAGE

PLEASE DO NOT RETURN YOUR FORM TO THE ABOVE ORGANIZATION.

1. REPORT DATE	2. REPORT TYPE	3. DATES COVERED	
20240213	Final	START DATE 20180701	END DATE 20220630

4. TITLE AND SUBTITLE
LOCAL MULTIPHYSICS STUDIES OF EPOXY NANOCOMPOSITES FOR ELECTRONICS PACKAGING

5a. CONTRACT NUMBER	5b. GRANT NUMBER	5c. PROGRAM ELEMENT NUMBER
	FA9550-18-1-0258	61102F
5d. PROJECT NUMBER	**5e. TASK NUMBER**	**5f. WORK UNIT NUMBER**

6. AUTHOR(S)
Ioannis Chasiotis

7. PERFORMING ORGANIZATION NAME(S) AND ADDRESS(ES)
UNIVERSITY OF ILLINOIS
506 S WRIGHT ST
URBANA, IL 61801
USA

8. PERFORMING ORGANIZATION REPORT NUMBER

9. SPONSORING/MONITORING AGENCY NAME(S) AND ADDRESS(ES)	10. SPONSOR/MONITOR'S ACRONYM(S)	11. SPONSOR/MONITOR'S REPORT NUMBER(S)
Air Force Office of Scientific Research 875 N. Randolph St. Room 3112 Arlington, VA 22203	AFRL/AFOSR RTB2	AFRL-AFOSR-VA-TR-2024-0156

12. DISTRIBUTION/AVAILABILITY STATEMENT
A Distribution Unlimited: PB Public Release

13. SUPPLEMENTARY NOTES

14. ABSTRACT
In the no-cost extension period of this project, we investigated the local micro- and nanoscale electrical properties of polydimethylsiloxane (PDMS) matrix composites with 12 wt% (below the electrical percolation threshold) and 20 wt% (above the electrical percolation threshold) carbon black (CB) nanoparticles in the range of 0-60% tensile strain with the aid of an Atomic Force Microscope (AFM) and a microtensile apparatus we developed in the previous reporting periods. A comparison of macroscale 2D finite strain fields with microscale strain fields, obtained from AFM images and digital image correlation, showed that 50×25 μm2 specimen domains were a representative element describing the effective mechanical response of the PDMS-CB nanocomposites. Similarly, 25×12 μm2 specimen domains provided consistent total current measurements as larger surface areas, thus serving as a representative element for the effective surface electrical response of PDMS-CB nanocomposites subjected to a broad range of strains. It was further shown that the transverse specimen contraction due to the Poisson's effect increased the initially low through-thickness electrical conductivity of PDMS with 12 wt% CB (below the electrical percolation threshold), with a rapid increase in the local electric current taking place above 30% applied strain, also resulting in a transition of the local surface conductivity from tunneling to a combination of Ohmic (linear I-V characteristic) and tunneling (non-linear I-V characteristic and lower electric current). On the other hand, the continuous reduction in the Poisson's effect, from ~0.5 at 0% strain to 0.25 at 60% strain, reduced the rate of increase of the effective local conductivity of PDMS composites with 20 wt% CB (above the electrical percolation threshold) with applied strain, with the vast majority of conductive surface sites demonstrating Ohmic behavior at 50% applied strain. The results of this research are important in multiscale and multiphysics modeling and simulations of soft nanocomposites, and in manufacturing of soft electrically conducting devices with feature sizes at the microscale, by providing quantitative inputs of the local and effective electrical response at different length scales.

15. SUBJECT TERMS

16. SECURITY CLASSIFICATION OF:			17. LIMITATION OF ABSTRACT	18. NUMBER OF PAGES
a. REPORT U	b. ABSTRACT U	c. THIS PAGE U	UU	22

19a. NAME OF RESPONSIBLE PERSON	19b. PHONE NUMBER *(Include area code)*
BYUNG LEE	426-8483

Standard Form 298 (Rev.5/2020)
Prescribed by ANSI Std. Z39.18

DISTRIBUTION A: Distribution approved for public release.

UNIVERSITY OF ILLINOIS
AEROSPACE ENGINEERING

Final Performance Report

Reporting Period: 07/01/2021 - 06/30/2022

(No-cost Extension)

Local Multiphysics Studies of Soft Nanocomposites

PI: Ioannis Chasiotis

Aerospace Engineering
University of Illinois at Urbana-Champaign
Talbot Lab, 104 S. Wright Street, Urbana, IL 61801
Telephone: (217) 244-1474, Fax: (217) 244-0720, E-mail: chasioti@illinois.edu

AFOSR Grant # FA9550-18-1-0258
Program Manager: Dr. B.L. "Les" Lee

July 8, 2022

DISTRIBUTION A: Distribution approved for public release.

REPORT DOCUMENTATION PAGE

Form Approved
OMB No. 0704-0188

Public reporting burden for this collection of information is estimated to average 1 hour per response, including the time for reviewing instructions, searching existing data sources, gathering and maintaining the data needed, and completing and reviewing this collection of information. Send comments regarding this burden estimate or any other aspect of this collection of information, including suggestions for reducing this burden to Department of Defense, Washington Headquarters Services, Directorate for Information Operations and Reports (0704-0188), 1215 Jefferson Davis Highway, Suite 1204, Arlington, VA 22202-4302. Respondents should be aware that notwithstanding any other provision of law, no person shall be subject to any penalty for failing to comply with a collection of information if it does not display a currently valid OMB control number. **PLEASE DO NOT RETURN YOUR FORM TO THE ABOVE ADDRESS.**

1. REPORT DATE *(DD-MM-YYYY)*	**2. REPORT TYPE**	**3. DATES COVERED** *(From - To)*
7/8/2022	FINAL PERFORMANCE REPORT	07/01/2021-06/30/2022

4. TITLE AND SUBTITLE

Local Multiphysics Studies of PDMS Based Nanocomposites for Electronics Packaging

5a. CONTRACT NUMBER

5b. GRANT NUMBER
FA9550-18-1-0258

5c. PROGRAM ELEMENT NUMBER

6. AUTHOR(S) IOANNIS CHASIOTIS

Aerospace Engineering, U. Illinois at Urbana-Champaign, M/C 236
306 Talbot Lab, 104 South Wright St., Urbana, IL 61801

5d. PROJECT NUMBER

5e. TASK NUMBER

5f. WORK UNIT NUMBER

7. PERFORMING ORGANIZATION NAME(S) AND ADDRESS(ES)

UNIVERSITY OF ILLINOIS
Aerospace Engineering
104 South Wright St.
Urbana, IL 61801

8. PERFORMING ORGANIZATION REPORT NUMBER

9. SPONSORING / MONITORING AGENCY NAME(S) AND ADDRESS(ES)

Air Force Office of
Scientific Research (AFOSR)
Program: Mechanics of
Multifunctional Materials and
Microsystems

10. SPONSOR/MONITOR'S ACRONYM(S)
Program Manager:
Dr. B.L. Lee

11. SPONSOR/MONITOR'S REPORT NUMBER(S)

12. DISTRIBUTION / AVAILABILITY STATEMENT
Approved for public release

13. SUPPLEMENTARY NOTES

14. ABSTRACT

In the no-cost extension period of this project, we investigated the local micro- and nanoscale electrical properties of polydimethylsiloxane (PDMS) matrix composites with 12 wt% (below the electrical percolation threshold) and 20 wt% (above the electrical percolation threshold) carbon black (CB) nanoparticles in the range of 0-60% tensile strain with the aid of an Atomic Force Microscope (AFM) and a microtensile apparatus we developed in the previous reporting periods. A comparison of macroscale 2D finite strain fields with microscale strain fields, obtained from AFM images and digital image correlation, showed that 50×25 μm^2 specimen domains were a representative element describing the effective mechanical response of the PDMS-CB nanocomposites. Similarly, 25×12 μm^2 specimen domains provided consistent total current measurements as larger surface areas, thus serving as a representative element for the effective surface electrical response of PDMS-CB nanocomposites subjected to a broad range of strains. It was further shown that the transverse specimen contraction due to the Poisson's effect increased the initially low through-thickness electrical conductivity of PDMS with 12 wt% CB (below the electrical percolation threshold), with a rapid increase in the local electric current taking place above 30% applied strain, also resulting in a transition of the local surface conductivity from tunneling to a combination of Ohmic (linear I-V characteristic) and tunneling (non-linear I-V characteristic and lower electric current). On the other hand, the continuous reduction in the Poisson's effect, from ~0.5 at 0% strain to 0.25 at 60% strain, reduced the rate of increase of the effective local conductivity of PDMS composites with 20 wt% CB (above the electrical percolation threshold) with applied strain, with the vast majority of conductive surface sites demonstrating Ohmic behavior at 50% applied strain. The results of this research are important in multiscale and multiphysics modeling and simulations of soft nanocomposites, and in manufacturing of soft electrically conducting devices with feature sizes at the microscale, by providing quantitative inputs of the local and effective electrical response at different length scales.

DISTRIBUTION A: Distribution approved for public release.

15. SUBJECT TERMS Multiphysics measurements, stretchable electronics, conductive elastomers, microscale testing, finite deformations, digital image correlation					
16. SECURITY CLASSIFICATION OF:			**17. LIMITATION OF ABSTRACT**	**18. NUMBER OF PAGES**	**19a. NAME OF RESPONSIBLE PERSON** Ioannis Chasiotis
a. REPORT unclassified	**b. ABSTRACT** unclassified	**c. THIS PAGE** unclassified		22	**19b. TELEPHONE NUMBER** *(include area code) (217) –244-1474*

Standard Form 298 (Rev. 8-98)
Prescribed by ANSI Std. Z39.18

DISTRIBUTION A: Distribution approved for public release.

Acknowledgements

The PI and his students supported by this grant gratefully acknowledge the support by the Air Force Office of Scientific Research (AFOSR) through grant FA9550-18-1-0258 with Dr. B.L. Lee as the program manager.

Publications

The following journal papers were derived from work done under this grant:

[1] K-K. Hung and I. Chasiotis, "Control of Substrate Strain Transfer to Thin Film Photovoltaics via Interface Design," Solar Energy **255**, pp. 643-655, (2021).

[2] K-K. Hung and I. Chasiotis, "Control of Surface Wrinkling through Compliant Nanostructured Interfaces," Advanced Materials Interfaces, **9**(3), pp. 2101583, (2022).

[3] O.E. Moronkeji, D. Das, S. Lee, K.M. Chang and I. Chasiotis, "Local Electrical Conductivity of PDMS-CB Nanocomposites Subjected to Large Deformations," in review, Journal of Composite Materials, (2022).

[4] D. Das, S. Lee, O.E. Moronkeji and I. Chasiotis, "Quantitative Fast and Full-field Measurements of Large Deformations by In-Situ Atomic Force Microscopy," in preparation, (2022).

DISTRIBUTION A: Distribution approved for public release.

FINAL TECHNICAL REPORT

This Final Progress Report summarizes the research conducted during the 12 months of no cost extension (NCE) of this grant. The research performed in the first three years of this project was described in detail in the three Annual Progress Reports submitted in the past.

1. INTRODUCTION

Highly compliant materials, such as polydimethylsiloxane (PDMS) [1] and Ecoflex [2], have received major attention in the recent years because of their large extensibility, outstanding stiffening properties at high stretch ratios, and excellent miscibility with a variety of fillers. The versatility in tuning the elastic modulus of PDMS from the kPa to the MPa range has enabled numerous possibilities for new devices and applications. The vast majority of elastomers are insulators with electrical surface resistivities of the order of 10^{12} Ω·cm [3]. The addition of electrically conductive nanomaterials, such as carbon nanotubes (CNTs) [4], carbon black (CB) [3], silver-coated carbon nanofibers [5] and liquid metals [6], has provided the means to tune the local and bulk electrical properties of elastomers to the antistatic and conductive ranges [3,7], thus, extending their applications to stretchable electronics [8,9], electronics packaging [10], strain sensors [11-15], etc. A difference between fibrous and particulate fillers is the electrical response of the resulting composites at larger deformations. Entangled networks of fibrous fillers (e.g. CNTs) support sustained electrical conductivities at large strains as opposed to spheroidal fillers (e.g. CB) [13] that rely on the formation of electrical percolation networks, which can be disrupted by the application of finite strains.

In the case of elastomers whose electrical conductivity is derived from the addition of conducting spherical particles, the filler material facilitates current flow either through a continuous network of filler particles, or a distribution of filler particles that allows for electron tunneling at small interparticle distances. In reality, the macroscopic conductivity is the outcome of a combination of the aforementioned mechanisms. Clearly, the first mechanism is the most desirable as it leads to repeatable and predictable behavior through an Ohmic behavior (linear I-V characteristics), but requires large filler volume fractions. Prior studies have shown that the bulk (volumetric) electrical conductivity of elastomers follows Ohmic behavior above the threshold for electrical percolation, namely the filler volume (or weight) fraction that results in drastically reduced resistivity [13-15]. However, even in electrically percolated elastomeric composites, not all conducting sites on the material surface would exhibit Ohmic behavior.

The electrical percolation threshold is smaller than the mechanical or geometric percolation thresholds, as a few filler networks are sufficient to form in the matrix to conduct

DISTRIBUTION A: Distribution approved for public release.

current, while tunneling (that does not require particle contact) can provide a measurable contribution to bulk conductivity. The electrical percolation threshold depends on the surface energies of the elastomer and the filler, the filler volume fraction and, importantly, the filler geometry. Compared to fibrous fillers such as aligned or entangled CNTs with percolation thresholds as small as 0.0025 wt% [16], equiaxed nanoparticles such as CB and silver nanoparticles [9,17] have much larger percolation thresholds ranging from 3 wt% for a few matrices [18] to 15-20 wt% for the majority of matrix materials [17,19]. Yet, while considerably larger amounts of CB are required for electrical percolation compared to CNTs, processability and cost considerations favor its use in conductive elastomers. Because of these considerations, the use of significant volume fractions of CB is common practice in a variety of elastomer matrices, such as PDMS for flexible and direct ink write (DIW) electronics, and polyvinylidene fluoride (PVDF) for battery electrodes [20].

While the bulk conductivity of conductive elastomers has been established both at the as-fabricated state and as a function of applied strain [13-15], the micron-scale local conductivity and its spatial distribution as a function of mechanical deformation remain elusive. The distribution and nature (Ohmic vs. tunneling) of local conductivity sites in a soft matrix are important parameters, both for predicting bulk conductivity and for determining the local variability of electrical properties in applications with component sizes and geometrical features at the submillimeter and the micrometer length scales. At the scale of CB inclusions, only contact Atomic Force Microscopy (AFM) can provide the local surface distribution of electric current via conductive AFM (C-AFM) imaging [21,22]. The few published studies utilizing conductive AFM [23-26] have shown that the conductive sites on the surface of polymeric materials are not uniformly Ohmic [24], with no straightforward correlation between local and bulk conductivity data. Furthermore, only one C-AFM study has examined the PDMS-CB system in the past, with all other studies focusing on as-fabricated unstrained composites. Yet, since the purpose of conductive elastomers is to enable the application of large strains, local conductivity studies under mechanical deformation are required but currently lacking. Mechanical deformation of the elastomeric matrix is expected to modify the conductive network of CB particles, hence resulting in microstructural evolution and changes in local conductivity, which, in turn, would be reflected in changes in bulk conductivity [13-15].

In this reporting period, the effect of applied strain on the local and bulk conductivity of PDMS-CB composite films was investigated along with local quantitative strain measurements with the aid of an AFM and Digital Image Correlation (DIC). This strain measurement methodology is based on prior AFOSR-supported research to resolve local deformation fields in heterogeneous materials [27-30]. Herein this methodology is extended to the application of finite (large) deformations with concurrent recording of local current at the scale of CB nanoparticles.

DISTRIBUTION A: Distribution approved for public release.

2. MATERIALS AND METHODS

2.a Specimen Fabrication

The PDMS matrix for this work was fabricated from a SYLGARD 184 silicone elastomer kit (Dow Corning, Midland, MI). High electrical conductivity CB with typical particle size <50 nm (Imerys C-NERGY SUPER C65, MSE Supplies, Tucson, AZ) served as the filler. CB was homogenously dispersed in toluene (Supelco) using a 1:15 CB-to-solvent weight ratio. The CB/toluene mixture was agitated with the aid of a homogenizer (OMNI-500 homogenizer, 120V 125W) for 5 min to induce agglomerate dispersion. The elastomer was then added to the mixture that was further agitated at 30,000 rpm for 5 min to obtain a homogenous mixture that was placed in a high-vacuum Schlenk for 12 hr at room temperature to evaporate the solvent, followed by 6 hr under a fume hood to further reduce the toluene content in the PDMS-CB mixture. The curing agent was then added to the CB/PDMS in a 10:1 PDMS:curing agent weight ratio and was vigorously hand-mixed. The final mixture was cast in dog-bone and straight beam shaped aluminum molds (fabricated via electrical discharge machining) to form 500-µm thick tensile specimens with 4 mm gauge length and 1 mm width. The cast specimens were oven-cured, first for 3 hr at 60 °C, followed by 1 hr at 100 °C. They were allowed to cool for 8 hr before removed from the molds. Three types of PDMS-CB specimens with 12 wt% and 20 wt% CB were prepared using this methodology. The particular CB weight fractions were selected based on literature reports for the same matrix-filler system that demonstrates a percolation threshold of 14-15% [14,15]. To limit the effect of contact resistance in electrical measurements, the PDMS-CB composites specimen surfaces that were attached to a bias probe were sputter-coated (Emscope SC 500) with a 60 nm layer of Au-Pd on the specimen grips or the bottom surface of the test specimens whose top surface was imaged with an AFM to obtain surface current maps.

2.b Mechanical and Electrical Measurements

All test specimens were preconditioned for 10 loading-unloading cycles before mechanical testing. A miniature apparatus, designed and built in a previous reporting period of this project, was employed for *in situ* mechanical testing while recording bulk and local electrical data [31]. The mechanical testing device, Figure 1(a), was designed to apply strains of 100% or larger. In the present experiments, the ultimate tensile strain of the CB composite specimens was almost always less than 100%. This mechanical testing device was utilized with an optical microscope for macroscale property measurements, and with an AFM (MFP3D, Asylum Research) to simultaneously record contact-AFM topography images and C-AFM data. To maintain compactness, the mechanical testing device was operated manually, which is sufficient, given the relatively long times (8 min) required to acquire a contact AFM image.

DISTRIBUTION A: Distribution approved for public release.

In-plane (2D) strain fields were extracted with the aid of DIC from 25×50 μm^2 surface topography AFM images and from optical images obtained from 1.5×2.00 mm^2 specimen areas under 50× optical magnification. The freestanding test specimens were attached to the apparatus grips with a 5-min two-part epoxy. As shown in Figure 1(a), each grip also served as a miniature folded beam loadcell. The force applied to a specimen was measured by monitoring the deflection of a pair of folded beams on each grip, serving as flexure loadcells, through an optical microscope at 50× optical magnification. During testing under an optical microscope, increments of force were applied and optical images of the specimen gauge section and the folded beam load cell were acquired. Application of DIC provided the displacement field in the specimen and the loadcell opening with subpixel resolution. This force measurement concept follows previous designs of MEMS microtools for mechanical testing developed by this group [32-35]. The loadcell force constant was calculated from its measured dimensions and also directly calibrated with the aid of a commercial low force loadcell as 18 mN/µm. All *in situ* AFM uniaxial tension experiments were conducted with preconditioned specimens. The specimen surface roughness served as a natural speckle pattern to carry out full-field strain calculations via DIC. Although possible, optical images were not obtained during *in situ* AFM mechanical testing to determine the applied force through the opening of the folded beam loadcell, because of the need for continuous repositioning of the testing device under the AFM. All AFM images were obtained at a scanning frequency of 1 Hz.

2.c AFM Methodology

For C-AFM measurements the PDMS-CB specimens were mounted on the apparatus for tensile testing with the aid of a two-part epoxy on one side while placing a metal plate on the top side of the Au-Pt coated specimen tab to establish electrical connection. A magnet was attached to the mechanical testing device to mount a bias wire to the test specimen. This was facilitated by the aluminum construction of the apparatus. Prior to mounting the mechanical testing device under the AFM, a multimeter was used to verify that the total apparatus and test specimen electrical resistance was the same as the specimen resistance.

Two types of AFM cantilevers for electrical conductivity measurements were tested: The first (ElectriMulti75-G, Budget Sensors) contained a rotated tip coated with 5 nm Cr and 25 nm Pt, resulting in 25-nm nominal tip radius (75 kHz resonance frequency, 3 N/m nominal force constant). The second type of cantilever (PPP-CONTSCPt, Nanosensors) was coated with 25 nm Cr and PtIr5 resulting in a nominal tip radius smaller than 25 nm (25 kHz resonance frequency, 0.2 N/m nominal force constant). A comparison of the surface topography and local current distribution on a specimen with 20 wt% CB, as obtained by the two cantilever types showed a relatively finer surface topography resolved by the PPP-CONTSCPt probe in a 50×50 μm^2 area (the contact force was the same for both types of AFM cantilevers), while the surface current

DISTRIBUTION A: Distribution approved for public release.

maps obtained by the two types of probes were virtually indistinguishable. Because the surface topography was utilized for DIC-based strain calculations, the PPP-CONTSCPt probe was selected for all imaging in this study.

While the resolution of surface topography is determined by the cantilever tip radius and image pixel size, the resolution of the conductive specimen area is determined by the pixel size for CB particles that are equal or smaller than the pixel size. Given that the CB particle size was ~50 nm [36] a minimum pixel size of 50 nm is required, which was used in this study. Furthermore, the use of an AFM tip with 25 nm radius implies sampling a circle with up to 50 nm diameter. Since the maximum sampling resolution of the AFM was 1024 pixels per scan line, an image area of 50×25 μm^2 was selected to avoid under-sampling, roughly corresponding to 1024×512 pixels. Thus, all AFM images obtained during tensile testing were rectangular (2:1 aspect ratio) with the long dimension oriented in the direction of specimen extension that results in the largest strain. This strategy reduced the AFM imaging time to half.

Finally, local I-V characteristics were obtained from CB surface particles located in 5×5 μm^2 subsets of the 50×25 μm^2 test areas, for a broad range of local current values determined through C-AFM. The force applied by the AFM tip to the sample was controlled during C-AFM to reduce the electrical contact resistance, and the cantilever force constant was determined by the thermal fluctuations method.

3. RESULTS AND DISCUSSION

3.a Local and Macroscale Mechanical Behavior

The mechanical response of pure PDMS and PDMS-CB specimens with 12 and 20 wt% CB obtained from *in situ* optical microscopy experiments is shown in Figure 1(b,c). Measurements were limited to <100% strain because of composite specimen failure at strains of the order of 80%, which is consistent with literature results for PDMS samples with similar CB loads [37,38]. For both CB weight fractions, Figures 1(b,c), the first two loading cycles exhibited a different mechanical response compared to all subsequent cycles that followed repeatable curves. Similarly, the bulk resistance and resistivity along the specimen required a preconditioning cycle to obtain consistent resistance measurements, Figures 2(a,b).

A direct comparison of longitudinal, ε_{xx}, and transverse, ε_{yy}, strains derived from macroscale (optical) and microscale (AFM) measurements is shown in Figure 1(d) by plotting the transverse-to-longitudinal strain ratio $-(\varepsilon_{yy}/\varepsilon_{xx})$ (equal to the Poisson's ratio for infinitesimal strains) as a function of the uniaxial strain, ε_{xx}. The two types of measurements agreed well at all applied strains, therefore, mechanically speaking the specimen domains of 50×25 μm^2 imaged by the AFM were sufficiently large to be representative of the macroscale mechanical behavior of PDMS-CB specimens and, thus, considered a Representative Surface Element (RSE).

DISTRIBUTION A: Distribution approved for public release.

As expected for an elastomer, for small strains $-(\varepsilon_{yy}/\varepsilon_{xx}) \approx 0.5$ that gradually decreased to ~0.2 at 100% applied strain. This effect of increasing stretch ratio on $-(\varepsilon_{yy}/\varepsilon_{xx})$ has been reported before for elastomers and elastomers with filler particles [39,40].

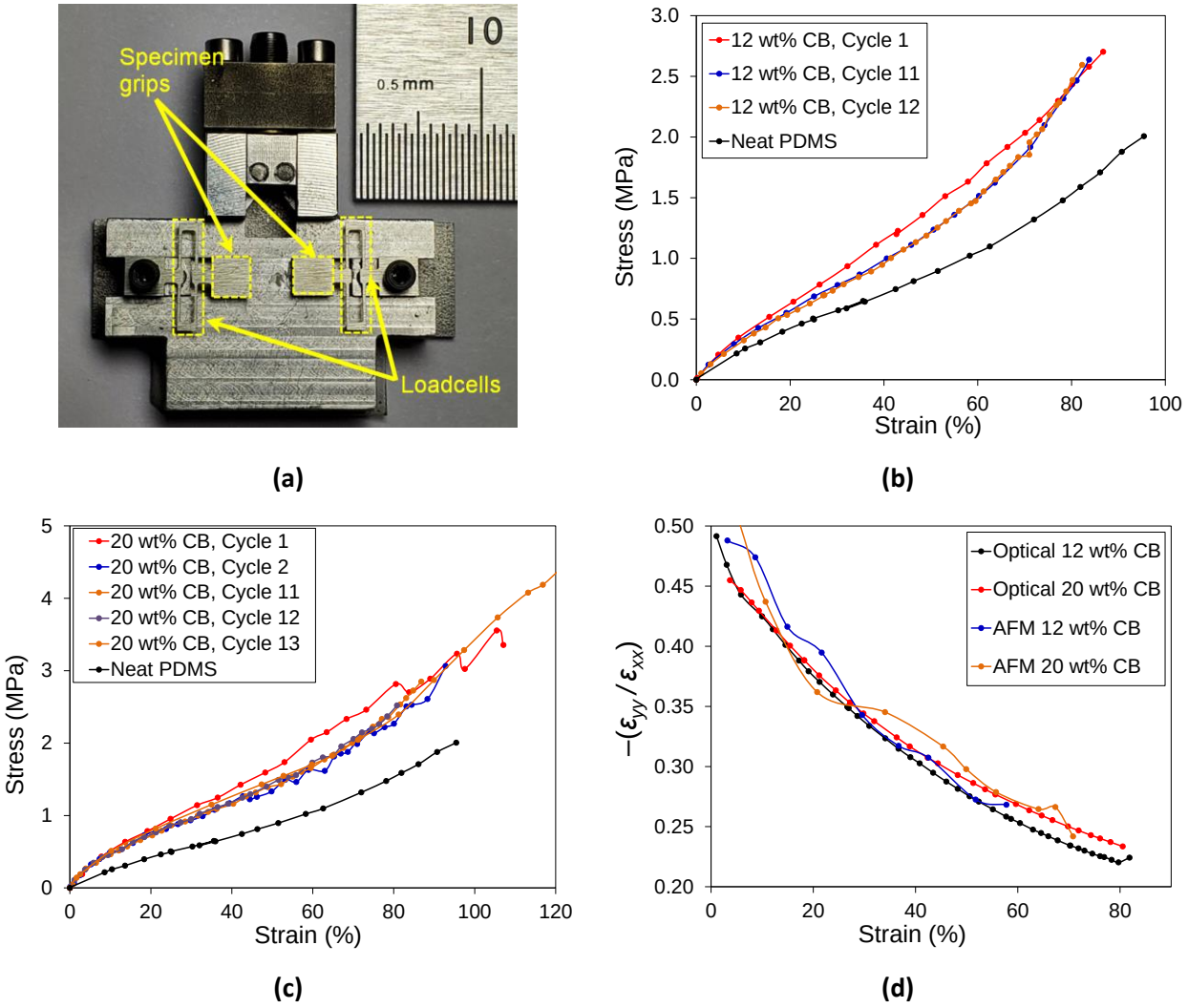

Figure 1. (a) Miniature mechanical testing device. The grips serve as force sensors in the form of folded beam loadcells as marked in the figure by the dashed lines. Changes in the opening of a folded beam are measured by an optical microscope and are used to calculate the applied force to the specimen. Stress-stain curves for **(b)** 12 wt% and **(c)** 20 wt% PDMS-CB composites. All curves are repeatable after the first two cycles. **(d)**. Ratio of transverse-to-longitudinal strain $[-(\varepsilon_{yy}/\varepsilon_{xx})]$ as a function of ε_{xx}, obtained via optical and AFM microscopy.

DISTRIBUTION A: Distribution approved for public release.

3.b Electrical Measurements on as-fabricated Specimens

The electrical behavior of PDMS-CB composites was evaluated in the as-fabricated state at the local and bulk scales after mechanical preconditioning. A steady increase in electrical resistance took place with increasing applied strain which was fully reversed upon unloading. The initial bulk resistance of specimens with 20 wt% CB was 13 times smaller than specimens with 12 wt% CB (270 Ω vs. 3.5 kΩ), Figures 2(a,b). For both CB weight fractions, the electrical resistance along the specimen increased non-linearly with applied strain as the CB particles were further separated upon specimen extension, reaching 360 Ω and 6 kΩ, respectively. A prior study has shown a dominant Ohmic response for CB weight fractions as low as 10% [14], while other works have reported a relatively linear dependence of the change in resistance as a function of applied strain, for CB weight fractions as small as 1% [14,15]. Similarly, the through-thickness resistance was measured as a function of applied strain. In the as-fabricated state, the through-thickness resistance was 470 Ω for 12 wt% CB and 38 Ω for 20 wt% CB. Notably, the electrical resistivity, $\rho=R\cdot A/L$, where R is the measured electrical resistance, A is the specimen cross-section and the L is the specimen length, decreased with applied strain for both CB weight fractions, with as-fabricated values of 100 Ω·cm and 7 Ω·cm for 12 wt% CB and 20 wt% CB, respectively. These resistivity values are in good agreement with values reported by Chong et al. [14] ranging from 116 Ω·cm for 10 wt% CB to 4.6 Ω·cm at 25 wt%.

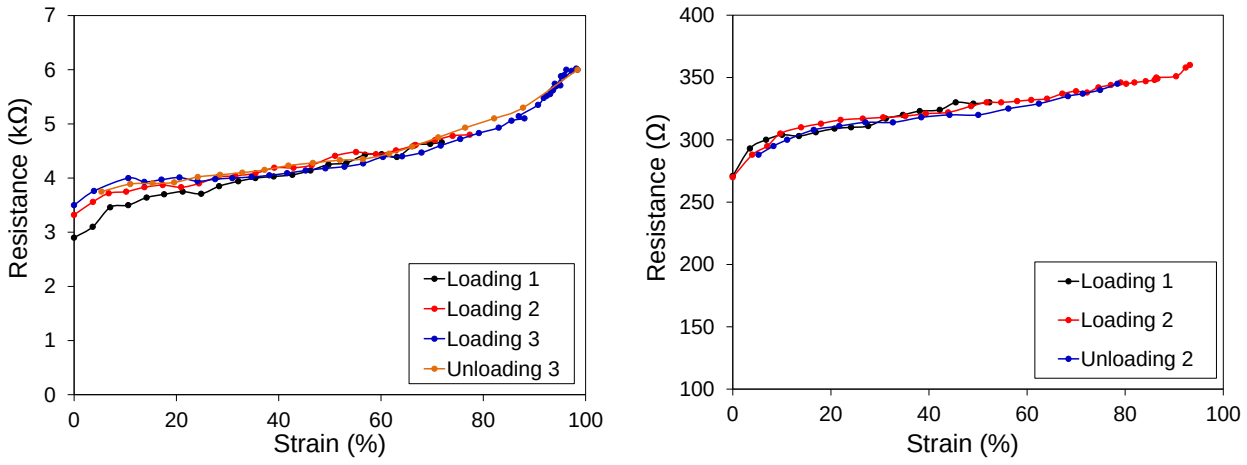

(a) **(b)**

Figure 2. Electrical resistance along the gauge length of **(a)** 12 wt%, and **(b)** 20 wt%, PDMS-CB specimens, as a function of applied uniaxial strain.

DISTRIBUTION A: Distribution approved for public release.

At the microscale, the electrical properties were quantified through local current maps obtained via C-AFM, which are representative of the through-thickness specimen conductivity (transverse to the direction of specimen stretching), as opposed to the measurements in Figures 2(a,b) that describe the bulk resistance along the direction of specimen stretching. The measured current depends on the local electrical conductivity and the contact resistance of the AFM tip and the sample surface. The contact resistance depends on the quality of the contact, which in the case of a CB particle in a highly deformable elastomeric substrate is expected to change significantly with the force applied by the AFM tip during contact imaging. Therefore, the effect of the AFM tip set point force on the total current was quantified using C-AFM current maps obtained at different bias voltages, Figures 3(a,b). Based on the C-AFM current maps the (i) conductive specimen area fraction, A_c, namely the area where current was measured (above the noise floor of 100 pA which was twice the current registered on C-AFM maps in PDMS regions of the specimen surface) was registered in AFM images divided by the total image area, and (ii) the total current, calculated by summing the current value at every C-AFM image pixel, which exceeded the current noise floor. A_c increased non-linearly with applied contact force, Figures 3(c,e), by a factor of 28, and 7 at the lowest applied voltage of 35 mV for 12 wt% and 20 wt% CB, respectively, and by a factor of 10, and 5 at the highest applied voltage of 2.5 V for 12 wt% and 20 wt% CB, respectively. It should be noted that for non-adhesive Hertzian contact the contact area, a, scales as $a \sim F^{1/3}$, namely the rapidly increasing A_c and total current with applied force is not due only to the increased contact area, rather mainly due to the reduced contact resistance. Similar were the trends in the total current as a function of applied force, Figures 3(d,f). While the higher the applied force, the smaller the contact resistance, the choice of the set point force for contact AFM imaging also took into account the surface distortion and AFM tip wear. It was found that imaging at 90 nN caused noticeable tip wear therefore, all contact AFM imaging in this study was carried out with 70 nN set point force, with 50 nN being the set point automatically assigned by the AFM software.

For both CB weight fractions A_c increased monotonically with applied voltage, Figures 3(c,e). Samples with 20 wt% CB demonstrated a linear behavior of A_c and total current as a function of applied voltage, Figure 3(f), which may be attributed to the fact that the CB content was above the percolation threshold; therefore most conducting sites are expected to be Ohmic. On the contrary, both A_c and the total current for specimens with 12 wt% CB were non-linear potentially due to a significant contribution of tunneling sites, since the 12 wt% PDMS-CB specimens were below the electrical percolation threshold. Local current-voltage (I-V) characteristics, obtained at selected points on the specimen surface, shed more light into local electrical conductivity. After full-field C-AFM imaging, local areas of 5×5 μm^2 were selected based on the C-AFM current maps to probe the electrical conductivity behavior of individual CB particles or agglomerates for applied bias voltage in the range ±0.25 V. These I-V characteristics are presented in Section 3.3 together with I-V curves obtained under specimen extension.

DISTRIBUTION A: Distribution approved for public release.

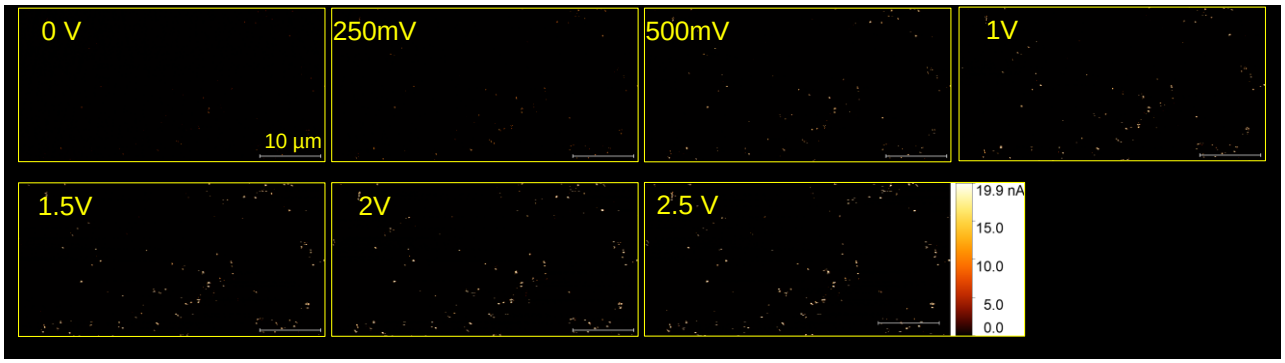

(a)

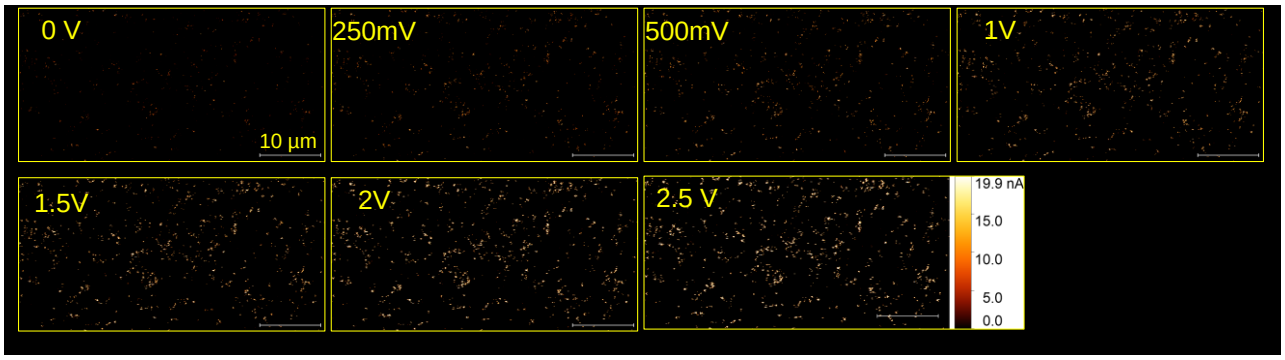

(b)

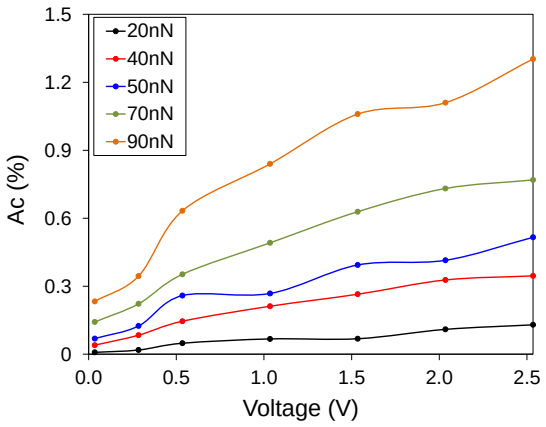

(c)

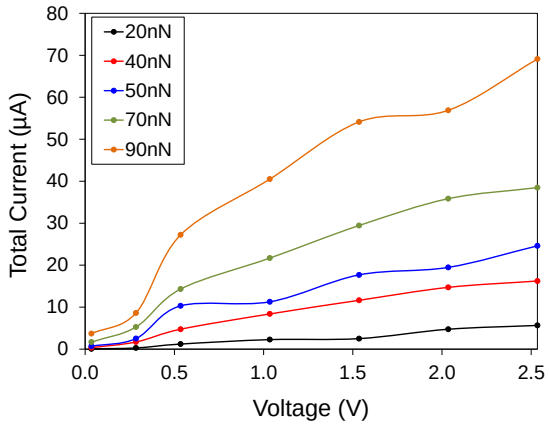

(d)

Figure continues on the next page

DISTRIBUTION A: Distribution approved for public release.

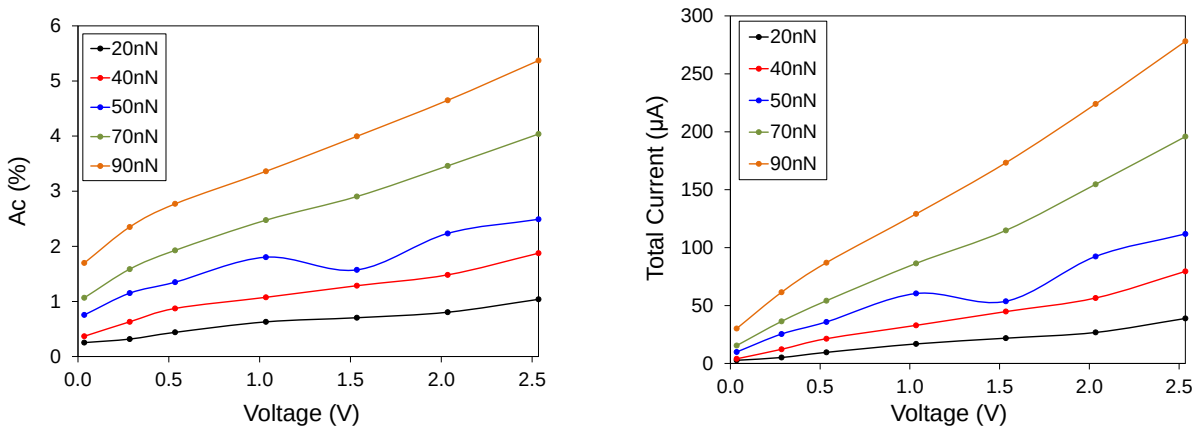

(e) **(f)**

Figure 3. Surface current maps obtained at 70 nN set point force for the AFM cantilever while imaging **(a)** 12 wt% and **(b)** 20 wt% PDMS-CB composites. **(c)** Conductive area fraction, A_c, (total area: 50×25 μm^2), and **(d)** total current of conductive areas in (a). **(e)** A_c (total area: 50×25 μm^2), and **(f)** total current of conductive areas in (b). A_c was calculated for pixels that exceeded the noise floor of 100 pA.

3.c Electrical Response under Uniaxial Tension

The evolution of conductive surface sites, local current distribution and total current were determined as a function of applied strain. Figures 4(a) and 4(b) show selected current maps in 12 wt% and 20 wt% PDMS-CB specimens, respectively, while Figures 4(c,d) are examples of the surface topography as the specimens were stretched. The entire set of current maps, similar to the sample images in Figures 4(a,b), was used to calculate the evolution of *Ac* and total current with applied strain, Figures 4(e,f), for the same undeformed area of 25×24 μm^2 marked with boxes in Figures 4(c,d), such that the electrical properties of the exact same physical surface points are tracked during mechanical deformation. In the case of 12 wt% CB, which is below the electrical percolation threshold, the total current followed a bi-linear trend with respect to the applied strain, while there was a relatively linear response in the case of 20 wt% CB, which is above the percolation threshold. Quantitatively speaking, at the applied strain of ~60% A_c was as high as 2.9% for the 12 wt% PDMS-CB specimen and 9.5% for the 20 wt% PDMS-CB specimen. Of similar magnitude, albeit not proportional to A_c, was the increase in total current at ~60% strain, reaching ~80 μA for the 12 wt% PDMS-CB specimen and 180 μA for the 20 wt% PDMS-CB specimen. The overall linearity in the total current vs. strain for the 20 wt% PDMS-CB specimen is due to a dominant Ohmic conductivity through the specimen thickness starting with the unstretched condition. On the contrary, the electrical conductivity of the 12 wt% PDMS-CB specimen is a combination of Ohmic conductance and electrical tunneling, hence resulting in the bilinear dependence on applied strain with a rapid increase of

DISTRIBUTION A: Distribution approved for public release.

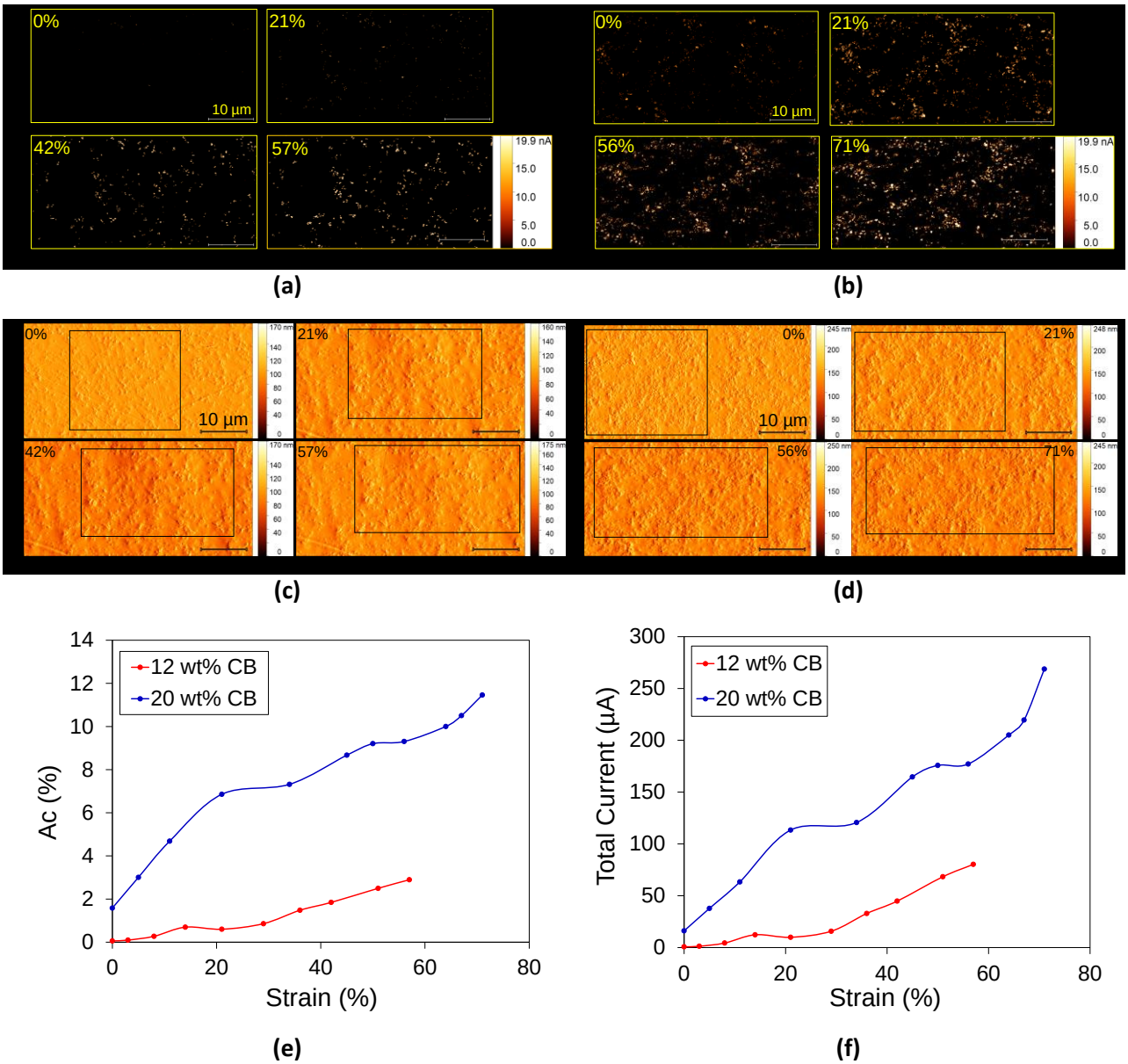

Figure 4. Current and surface topography AFM maps for a **(a,c)** 12 wt% and a **(b,d)** 20 wt% PDMS-CB specimen subjected to different applied uniaxial strain, ε_{xx}, values and 70 nN set point force. The boxed areas in the topography images in (c,d) correspond to the same undeformed 25×24 µm^2 area undergoing extension in x-direction and contraction in the y-direction during macroscale uniaxial tension. The current maps in (a) and (b) correspond to the same physical areas as the surface topography images in (c) and (d), respectively. **(e)** Fraction of conductive specimen area and **(f)** total current of conductive area as a function of uniaxial strain for 12 wt% and 20 wt% PDMS-CB specimens, calculated from the boxed areas in (c) and (d). The scale bars in (a-d) are equal to 10 µm.

DISTRIBUTION A: Distribution approved for public release.

the total current beyond 30% applied strain, Figure 5(a). The latter could be attributed to the reduction in specimen thickness due to Poisson's effect, thus causing a gradual transition to electrical percolation through the specimen thickness due to a reduction in CB particle spacing. Different trends were obtained for the 20 wt% PDMS-CB specimen, Figure 5(b): Overall, the total current per unit area increased following a rather bilinear response, with a reduced rate of increase after ~20% strain. The origins of this behavior may be traced in the gradually reduced rate of Poisson's contraction with applied strain, as shown in Figure 1(d), resulting in a decreasing rate of specimen contraction across its thickness combined with the increasing effect of longitudinal stretching on CB particle separation.

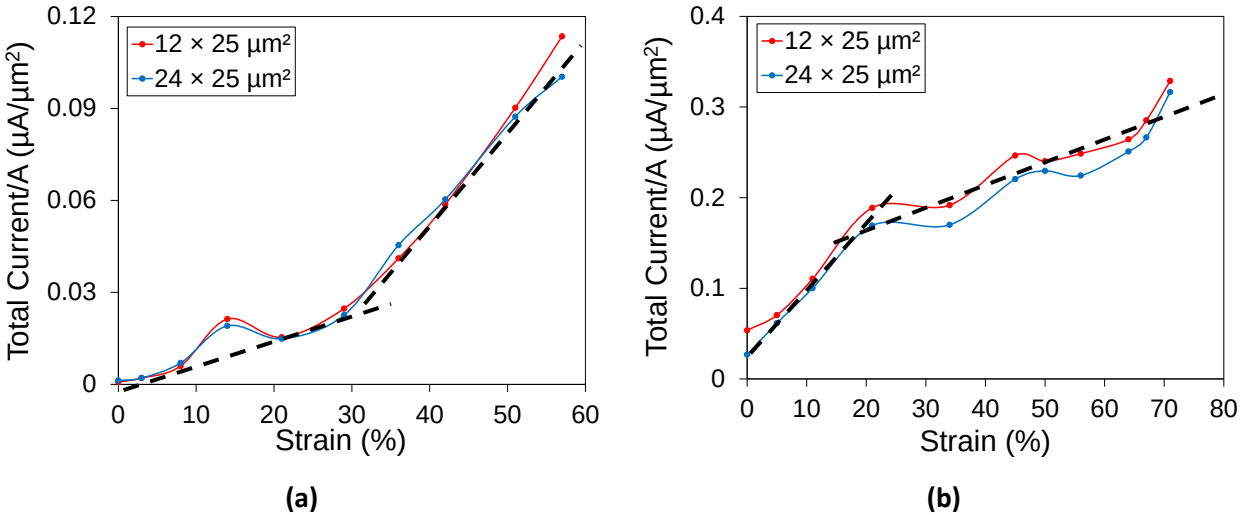

Figure 5. Total current per unit area vs. uniaxial strain for a **(a)** 12 wt% and a **(c)** 20 wt% PDMS-CB specimen, for two specimen areas whose local conductivity characteristics and dimensions were tracked during specimen stretching.

It is important to assess whether the C-AFM current maps in Figures 4(a,b) included a sufficient number of CB particles to be considered an RSA for electrical properties. Towards this goal, the total current per unit area was compared between specimen domains with initial dimensions of 25×24 μm^2 and 25×12 μm^2, which were tracked during deformation, as shown in Figures 4(c,d) for the 25×24 μm^2 area of interest (the 25×12 μm^2 area was the upper half of the region marked by a box in the AFM images for 0% strain), and plotted in Figures 5(a,b). In the case of the 12 wt% PDMS-CB specimen, the total current per unit area did not vary with the size of the imaging area during deformation. The total current per unit area for the 20 wt% PDMS-CB specimen did show a small difference between 25×24 μm^2 and 25×12 μm^2 areas, but small enough to characterize the 25×24 μm^2 surface area as an RSA for both types of PDMS-CB specimens.

DISTRIBUTION A: Distribution approved for public release.

Although there is no direct means to compare the macroscale electrical conductivity with the local C-AFM measurements, of further interest is to explore the nature of the conducting sites resolved in C-AFM maps through their I-V characteristics. Figures 6(a-d) show several I-V characteristics spanning a range of responses, obtained from undeformed specimens, and specimens that were deformed to 50% macroscale strain. Noting that the specimens with 12 wt% CB were below the electrical conductivity percolation threshold, the vast majority of I-V characteristics from the undeformed specimen in Figure 6(a) demonstrated the characteristic parabolic shape of tunneling conductance with a rapid increase in conductivity at higher bias voltage. This I-V response changed notably at 50% applied strain, Figure 6(b), where a combination of linear response, corresponding to Ohmic conductance, and non-linear response resulting in lower current, corresponding to tunneling, was recorded. This transition to significant degree of Ohmic conductance is in agreement with the rapid increase in the total current per unit area taking place beyond 30% applied strain, Figure 5(a), as calculated from the C-AFM maps and shown in Figure 4(a). On the other hand, the I-V characteristics of undeformed specimens with 20 wt% CB, Figure 6(c), were a combination of linear (Ohmic) and non-linear (tunneling). This behavior changed significantly upon application of 50% strain resulting in the majority of the probed cites responding Ohmically, Figure 6(d). The Poisson's contraction across the specimen thickness favors an increase in CB particle contact and, therefore, increased Ohmic-type conductance. Yet, there were still many locations of low current (100s of pA) compared to the Ohmic areas that provided >10 nA. Therefore, even after applying significant strain to already percolated specimens, the local conductivity characteristics remained a combination of (dominant) Ohmic and tunneling.

As a final note, although the insets of C-AFM current maps in Figures 6 show some CB clustering at the scale of 5×5 μm^2, the I-V characteristics at different locations of the same CB cluster were not constant, e.g. locations 1, 3, 5, 6 in the same large cluster in Figure 6(c), yielding either Ohmic or tunneling conductivity, hence indicating significant discontinuities within the same CB cluster. On the other hand, different points in much smaller CB clusters did demonstrate identical I-V characteristics, as shown in Figure 6(f). It is therefore concluded that the local conductivity mode at the scale of a few microns is highly non-uniform, even for specimens with CB weight fractions well above the electrical percolation threshold.

DISTRIBUTION A: Distribution approved for public release.

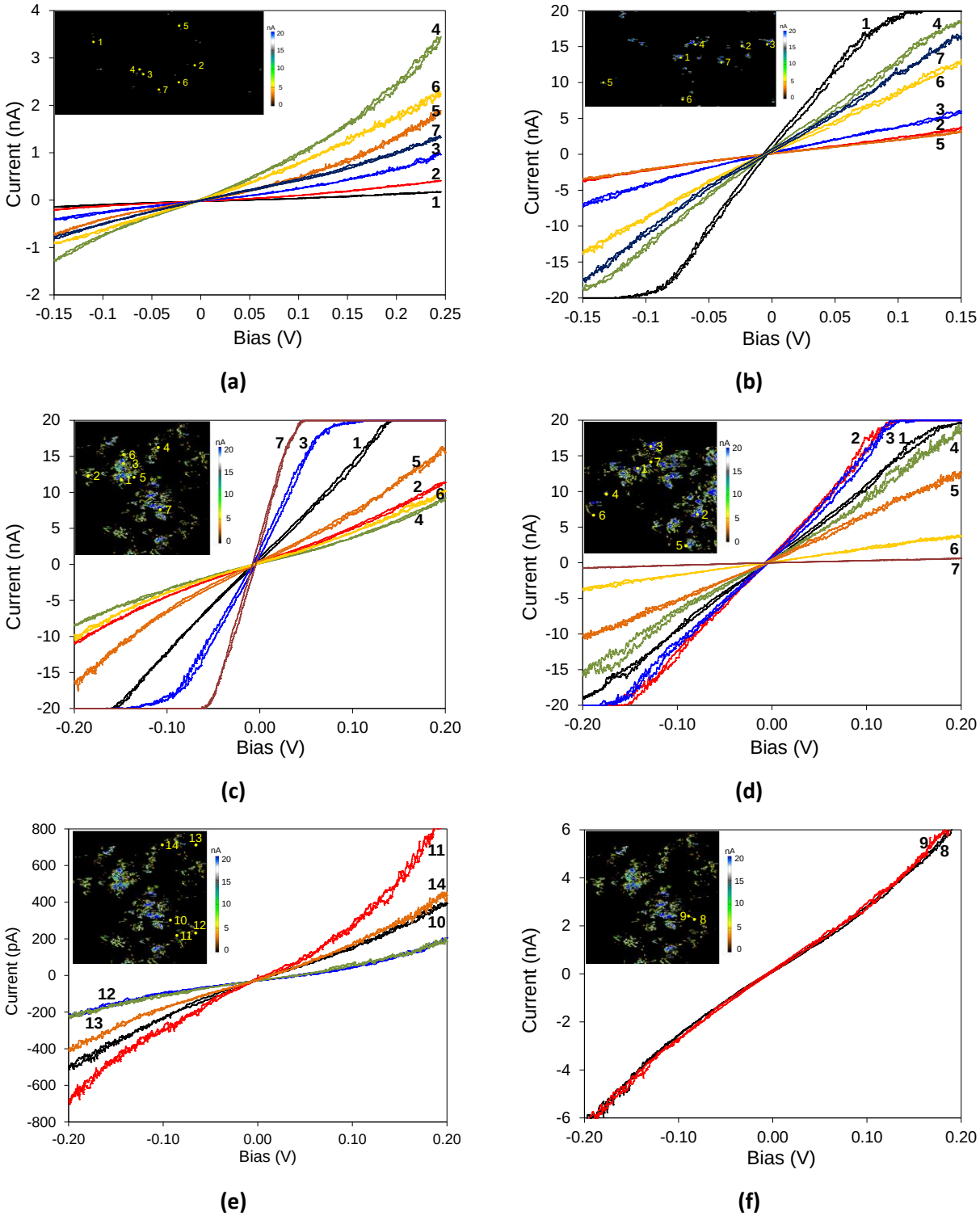

Figure 6. I-V characteristics from **(a,b)** 12 wt% and **(c-f)** 20 wt% PDMS-CB specimens subjected to **(a,c,e,f)** 0% and **(b,d)** 50% strain. **(e)** Low current I-V characteristics demonstrating tunneling behavior. **(f)** Identical I-V characteristics obtained along a chain of CB particles. The C-AFM insets in (a,b) are 10×20 μm^2 and in (c-f) are 5×5 μm^2.

DISTRIBUTION A: Distribution approved for public release.

4. CONCLUSIONS

The microscale electrical properties of PDMS-CB nanocomposites with CB compositions below (12 wt%) and above (20 wt%) the electrical percolation threshold were investigated under the application of large tensile strains. Background work showed that the contact resistance could be reduced quite significantly by increasing the set point force in contact AFM imaging albeit at the cost of rapid AFM tip wear. For specimens with a CB weight fraction below the electrical percolation threshold, it was shown that the rate of increase in electric current area density (in specimen domains of 25×25 μm^2) with applied strain surged beyond a threshold strain and the dominant local conductivity gradually assumed Ohmic characteristics, yet remaining a combination of Ohmic and tunneling-based. On the contrary, for specimens with a CB weight fraction above the electrical percolation threshold, the rate of increase in the electric current area density decreased beyond a threshold strain. The local conductance of specimens with 12 and 20 wt% CB was a combination of Ohmic and tunneling, with the former prevailing at large applied strains. The results of this work are important in multiscale and multiphysics modeling and simulations of soft nanocomposites and in manufacturing of soft electrically conducting devices with microscale feature sizes, by providing quantitative inputs about the local and effective electrical response at different length scales.

DISTRIBUTION A: Distribution approved for public release.

5. REFERENCES

[1] I. Teixeira, I. Castro, V. Carvalho, C. Rodrigues, A. Souza, R. Lima, S. Teixeira, J. Ribeiro, "Polydimethylsiloxane mechanical properties: A systematic review." *AIMS Materials Science,* **8**(6), pp. 952-973, (2021).

[2] D. Steck, J. Qu, S.B. Kordmahale, D. Tscharnuter, A. Muliana, J. Kameoka, "Mechanical responses of Ecoflex silicone rubber: Compressible and incompressible behaviors." *Journal of Applied Polymer Science*, **136(**5), pp. 47025, (2019).

[3] M.E. Spahr, R. Gilardi, D. Bonacchi, "Carbon black for electrically conductive polymer applications." Fillers for Polymer Applications, *Encyclopedia of Polymers and Composites*, pp 375-395, (2016).

[4] H. Wu, K. Wang, Y. Meng, K. Lu, Z. Wei, "An organic cathode material based on a polyimide/CNT nanocomposite for lithium ion batteries," *Journal of Materials Chemistry A*, **1**(1), pp. 6366-6372, (2013).

[5] F. Manea, S. Motoc, A. Pop, A. Remes, J. Schoonman, "Silver-functionalized carbon nanofiber composite electrodes for ibuprofen detection," *Nanoscale Research Letters*, **7**(1), pp. 331, (2012).

[6] C. Pan, E. J. Markvicka, M. H. Malakooti, J. Yan, L. Hu, K. Matyjaszewski, C. Majidi, "A Liquid-Metal-Elastomer Nanocomposite for Stretchable Dielectric Materials," *Advanced Materials*, **31**(23), p. 1900663, (2019).

[7] J. Markarian, "New developments in antistatic and conductive additives." *Plastics, Additives and Compounding*,**10**(5), pp. 22-25, (2008).

[8] J.A. Rogers, T. Someya, Y. Huang, "Materials and Mechanics for Stretchable Electronics," *Science*, **327**(5973), pp. 1603-1607, (2010).

[9] A. Larmagnac, S. Eggenberger, H. Janossy, J. Vörös, "Stretchable electronics based on Ag-PDMS composites." Scientific reports **4**(1), pp. 1-7, (2014).

[10] S.K. Bhattacharya, R.R. Tummala, "Integral passives for next generation of electronic packaging: application of epoxy/ceramic nanocomposites as integral capacitors," *Microelectronics Journal*, **32**(1), pp. 11-19, (2001).

[11] R. Zhang, H. Deng, R. Valenca, J. Jin, Q. Fu, E. Bilotti, T. Peijs, "Strain sensing behaviour of elastomeric composite films containing carbon nanotubes under cyclic loading," *Composites Science and Technology*, **74**(24), pp. 1-5, (2013).

[12] J-H. Kong, N-S. Jang, S-H. Kim, J-M. Kim. "Simple and rapid micropatterning of conductive carbon composites and its application to elastic strain sensors." *Carbon*, **77**, pp. 199-207, (2014).

[13] N. Lu, C. Lu, S. Yang, J. Rogers. "Highly sensitive skin-mountable strain gauges based entirely on elastomers." *Advanced Functional Materials*, **22**, no. 19, pp. 4044-4050, (2012).

[14] H. Chong, J. Lou, K.M. Bogie, C.A. Zorman, S.J.A. Majerus. "Vascular Pressure–Flow Measurement Using CB-PDMS Flexible Strain Sensor." *IEEE transactions on biomedical circuits and systems*, **13**, no. 6, pp. 1451-1461, (2019).

[15] X. Cheng, C. Bao, X. Wang, W. Dong. "Stretchable strain sensor based on conductive polymer for structural health monitoring of high-speed train head." *Proceedings of the Institution of Mechanical Engineers, Part L: Journal of Materials: Design and Applications*, **234**, no. 3, pp. 496-503, (2020).

[16] J.K.W. Sandler, J.E. Kirk, I.A. Kinloch, M.S.P. Shaffer, A.H. Windle. "Ultra-low electrical percolation threshold in carbon-nanotube-epoxy composites." *Polymer*, **44**, no. 19, pp. 5893-5899, (2003).

DISTRIBUTION A: Distribution approved for public release.

[17] X.Z. Niu, S.L. Peng, L.Y. Liu, W.J. Wen, P. Sheng, "Characterizing and patterning of PDMS-based conducting composites." *Advanced Materials*, **19**(18), pp. 2682-2686, (2007).

[18] S.R. Athreya, K. Kalaitzidou, S. Das, "Processing and characterization of a carbon black-filled electrically conductive Nylon-12 nanocomposite produced by selective laser sintering," *Material Science and Engineering: A*, **527**(10-11), pp. 2637-2642, (2010).

[19] J.-C. Huang, "Carbon black filled conducting polymers and polymer blends." *Advances in Polymer Technology: Journal of the Polymer Processing Institute* **21**(4), pp. 299-313, (2002).

[20] D. Antartis, S. Dillon, I. Chasiotis, "Effect of Porosity in Electrochemical and Mechanical Properties of Composite Li-ion Anodes", *Journal of Composite Materials* **49**, pp. 1849-1862, (2015).

[21] https://afm.oxinst.com/assets/uploads/products/asylum/documents/ORCA%E2%84%A2-%E2%80%93-Conductive-AFM-Imaging-Using-the-MFP-3D%E2%84%A2-AFM.pdf (Accessed on June 4, 2022).

[22] https://www.bruker.com/en/products-and-solutions/microscopes/materials-afm/afm-modes/c-afm.html (Accessed on June 4, 2022).

[23] R. Viswanathan, M.B. Heaney, "Direct imaging of the percolation network in a three-dimensional disordered conductor-insulator composite", *Physical review letters*, **75**(24), pp. 4433-4436, (1995).

[24] A. Alekseev, T.H. Wu, L.G.J. van der Ven, R.A.T.M. van Benthem, G. de With, "Global and local conductivity in percolating crosslinked carbon black/epoxy–amine composites," *Journal of Materials Science*, **55**(21), pp. 8930-8939, (2020).

[25] N. Shimoni, D. Azulay, I. Balberg, O. Millo. "Voltage induced electrical connectivity on a percolation cluster," *Physica Status Solidi* (b), **230**(1), pp. 143-150, (2002).

[26] A. Trionfi, D.A. Scrymgeour, J.W.P. Hsu, M.J. Arlen, D. Tomlin, J.D. Jacobs, D.H. Wang, L.-S. Tan, R.A. Vaia, "Direct imaging of current paths in multiwalled carbon nanofiber polymer nanocomposites using conducting-tip atomic force microscopy", *Journal of Applied Physics*, **104**(8), pp. 083708, (2008).

[27] S.W. Cho, I. Chasiotis, T.A. Friedmann, J. P. Sullivan. "Young's modulus, Poisson's ratio and failure properties of tetrahedral amorphous diamond-like carbon for MEMS devices." *Journal of Micromechanics and Microengineering*, **15**, no. 4 (2005): 728.

[28] S.W. Cho, I. Chasiotis, "Elastic Properties and Representative Volume Element of Polycrystalline Silicon for MEMS," *Experimental Mechanics* **47** (1), pp. 37-49, (2007).

[29] Q. Chen, I. Chasiotis, C. Chen, A. Roy, "Nanoscale and Effective Mechanical Behavior and Fracture of Silica Nanocomposites," *Composites Science and Technology,* **68**, pp. 3137-3144, (2008).

[30] S.W. Cho, K. Jonnalagadda, I. Chasiotis. "Mode I and mixed mode fracture of polysilicon for MEMS.", *Fatigue & Fracture of Engineering Materials & Structures*, **30**, no. 1 (2007): 21-31.

[31] D. Das, S. Lee, O.E. Moronkeji, I. Chasiotis, "Quantitative Fast and Full-field Measurements of Large Deformations by In-Situ Atomic Force Microscopy", *Scientific Reports*, in preparation, (2022).

[32] M. Naraghi, I. Chasiotis, Y. Dzenis, Y. Wen, H. Kahn, "Novel Method for Mechanical Characterization of Polymeric Nanofibers", *Review of Scientific Instruments*, **78**, pp. 085108, (2007).

[33] M. Naraghi, I. Chasiotis, "Optimization of Comb-driven Devices for Mechanical Testing of Polymeric Nanofibers Subjected to Large Deformations" *Journal of Microelectromechanical Systems*, **18**(5), pp. 1032-1046, (2009).

[34] D. Das, I. Chasiotis. "Sliding of adhesive nanoscale polymer contacts." *Journal of the Mechanics and Physics of Solids*, **140**, p. 103931, (2020).

DISTRIBUTION A: Distribution approved for public release.

[35] K. Sahin, N.A. Fasanella, P.V. Kolloru, I. Chasiotis, “Mechanical Property Experiments with Ultra-High Strength Micrometer Scale Fibers,” *Experimental Mechanics*, **55**, pp. 877-885, (2015).

[36] https://www.msesupplies.com/collections/cathode-materials/products/super-c65-carbon-black-conductive-additive-for-lithium-ion-battery-cathode-and-anode-50g?variant=31262541709370 (Accessed on June 4, 2022).

[37] C.B Karuthedath, U. Fikri, F. Ruf, N. Schwesinger. "Characterization of carbon black filled PDMS-composite membranes for sensor applications." *In Key engineering materials*, vol. **753**, pp. 18-27, Trans Tech Publications Ltd, (2017).

[38] H. Shivashankar, R. Sangamesh, S. M. Kulkarni. "Processing and investigation of mechanical characteristics on the polydimethylsiloxane/carbon black composites." *Materials Research Express*, **6**, no. 10, pp. 105340, (2019).

[39] H.P. Kugler, R.G. Stacer, C. Steimle. "Direct measurement of Poisson's ratio in elastomers." *Rubber chemistry and technology*, **63**, no. 4, pp. 473-487, (1990).

[40] T.L. Smith, "Volume changes and dewetting in glass bead-polyvinyl chloride elastomeric composites under large deformations." *Transactions of the Society of Rheology*, **3**, no. 1, pp. 113-136, (1959).

DISTRIBUTION A: Distribution approved for public release.